Journal of Asian Earth Sciences 239 (2022) 105405

Contents lists available at ScienceDirect

Journal of Asian Earth Sciences

journal homepage: www.elsevier.com/locate/jseaes

Bimodal distribution of amphibole-melt apparent dihedral angles in the product of the early crystallization of hydrous basaltic melts

Qizhe Tang [a], Bo Zhang [b,*], Wenge Zhou [c]

[a] School of Information Engineering, Huzhou University, Huzhou 313000, China
[b] Tourism Management School, Guizhou University of Commerce, Guiyang 550014, China
[c] Key Laboratory of High-Temperature and High-Pressure Study of the Earth's Interior, Institute of Geochemistry, Chinese Academy of Sciences, Guiyang 550081, China

ARTICLE INFO

Keywords:
Apparent dihedral angle
Anisotropic mineral
Early crystallization
Bimodal distribution
High pressure and high temperature

ABSTRACT

The dihedral angle of mineral-melt is a very important parameter for further understanding the textural evolution of magma crystallization. In this study, we have investigated the amphibole-melt dihedral angle distribution of four previous experimental samples at 0.6 GPa and 970 °C with annealing time of 1 h, 10 h, 60 h, and 100 h, as well as two additional experiments with annealing time of 5 h and 30 h. In this experiment, we have achieved the assemblage of amphibole + granodioritic melt ± traces of other minerals in the process of melt crystallization under the above experimental conditions. The apparent dihedral angles of amphibole-melt of the experimental products were obtained by randomly measuring the dihedral angles in the backscattered images. The results indicate that the apparent dihedral angle presents a gradually obvious bimodal distribution with the increasing annealing time. The high anisotropy of amphibole is believed to be the main cause of the bimodal characteristics of the apparent dihedral angle distribution. Consequently, two Gauss functions are used to fit one distribution. As the annealing time increases, the median-standard deviation relationships of the apparent dihedral angle for these two Gauss functions show great differences. Therefore, our experiments proved that in the amphibole-melt system, the median-standard deviation with the growth of textural equilibrium in the early crystallization is no longer a unidirectional change. Furthermore, combining the results of this study and the previous work, whether the dihedral angle distribution in the early crystallization is unimodal or bimodal may have great relationship with the anisotropy of minerals.

1. Introduction

The textures of rocks and crystals can convey a great deal of petrologic information. Particularly, the dihedral angle distribution in the solid-melt system is a key factor to study the texture evolution in igneous rocks (Holness, 2005; Ikeda et al., 2002).

Given the importance of the dihedral angle to the rock texture, there have been many attempts to quantify the dihedral angle of geological interest. Previous studies have presented the variation of mineral-melt dihedral angle during the evolution of magma crystallization by natural samples or experimental products under high-pressure and high-temperature (Bulau et al., 1979; Holness et al., 2006; Holness et al., 2007; Vicenzi et al., 1988; Waff and Bulau, 1979; Wolf and Wyllie, 1991), the results explained the evolution of the rock texture in the process of magma emplacement or volcanic eruption efficiently. For example, according to Holness et al. (2005), dihedral angles would reflect a departure from texture equilibrium, that a low median solid-melt-solid dihedral angle and low standard deviation was usually resulted in the melt-bearing equilibrium, while the solid-state equilibrium often resulted in a high median angle and low standard deviation. Furthermore, the lower dihedral angles may highly correlate to the presence of water in the olivine and plagioclase in basic and silicic magma systems, thus reflecting the enhancement of diffusion and equilibration rates with some control of pore geometry by crystal growth (Holness et al., 2005).

However, the early stage of crystallization process in the magma chamber is believed to be a process that gradually approaches equilibrium in almost constant pressure and temperature environment. To our knowledge, there have been few isothermal experiments at high pressure to investigate the relationship between the mineral-melt dihedral angle and crystallization time in the early stage of magma crystallization (Holness et al., 2019). Therefore, the details of textural development in

* Corresponding author.
E-mail address: 201910790@gzcc.edu.cn (B. Zhang).

https://doi.org/10.1016/j.jseaes.2022.105405
Received 25 June 2022; Received in revised form 9 September 2022; Accepted 12 September 2022
Available online 18 September 2022

the early stage of crystallization to the texture equilibrium have not been revealed by experiments under high temperature and high pressure.

Moreover, minerals with medium to low symmetry usually have anisotropic characteristics, which affects the anisotropic characteristics of minerals and the dihedral angle distribution of the mineral-melt. However, in the previous studies, the dihedral angle distribution of mineral-melt often conforms to a normal distribution, which may indicate that the influence of crystal anisotropy on the dihedral angle distribution of mineral-melt is almost negligible (Elliott et al., 1997; Holness, 2005; Jurewicz and Jurewicz, 1986). Hence, whether the crystal anisotropy has an effect on dihedral angle distribution is still unclear.

The present study deals with the early stage of amphibole crystallization in the hydrous basaltic melt by investigating the amphibole-melt dihedral angle distribution of four isothermal experimental samples of Zhang et al. (2019) at 0.6 GPa and 970 °C with the annealing time of 1 h, 10 h, 60 h and 100 h, as well as two additional isothermal experiments with annealing time of 5 h and 30 h. One of the most significant discoveries in the present study is the bimodal distribution of amphibole-melt dihedral angle with increasing annealing time. In addition, the origin of the bimodal distribution of amphibole-melt dihedral angle and the texture development in the early stage of magma crystallization are also discussed in the follow-up sections.

2. Experiments

2.1. High-pressure and high-temperature experiments

Starting materials for crystallization experiment comes from the Yichuan-Ruyang region in west Henan province, China, a natural basalt with modal mineralogy plagioclase (40 %), iddingsitized olivine (25 %), clinopyroxene (20 %), glass (10 %), and minor iron titanium oxide (5 %), the same as those by Zhang et al. (2019). After grinding and drying, the sample was encapsulated in graphite with pyrophyllite cube pressure medium for high-pressure and high-temperature experiments.

High-pressure and high-temperature experiments were carried out in the multi-anvil apparatus of YJ-3000t in the Key Laboratory for High-Temperature and High-Pressure Study of the Earth's Interior of the Institute of Geochemistry, Chinese Academy of Sciences. The accuracy of experimental pressure and temperature were ±0.05 GPa and ±5 °C, respectively. After experiment procedure of Zhang et al., (2019), two additional supplementary crystallization experiments were carried out and annealed for 5 h and 30 h at 0.6 GPa and 970 °C. In these two experiments, charges were held at 0.6 GPa and 1460 °C for 1 h, then rapidly cooled isobarically to the crystallization temperature of 970 °C, and held for 5 h or 30 h before quenching. Finally, samples were quenched by shutting off the electric power. The experimental conditions of these two experiments, along with the experiments with different annealing time of Zhang et al. (2019) are shown in Table 1. Detailed experimental processes are referred to (Zhang et al., 2019).

Table 1
Experimental conditions and phase compositions of run products.

Run	1[a]	2	3[a]	4	5[a]	6[a]
T(°C) [b]	1460/970	1460/970	1460/970	1460/970	1460/970	1460/970
P(GPa)	0.6	0.6	0.6	0.6	0.6	0.6
Annealing time (h)	1	5	10	30	60	100
Phase [c]	Amp + Ab + Apa + Melt	Amp + Melt	Amp + Apa + Melt	Amp + Melt	Amp + Apa + Melt	Amp + Apa + Melt

Abbreviations of phases: *Amp* amphibole, *Apa* apatite, *Ab* albite, *Melt* melt.
[a] Runs of 1, 3, 5, and 6 corresponds to experiments of 10084-8, 10084-9, 10084-10, and 10084-3 from Zhang et al. (2019), respectively.
[b] 1460/970 should be read as the melting temperature of 1460 °C and the crystallization temperature of 970 °C. See text for more details.

2.2. Analytical techniques and dihedral angle measurement

Backscattering (BSE) images of experimental products were performed on EPMA-1600 electron microprobe, the phase compositions were analyzed with JEOL JXA-8100 electron microprobe at the Institute of Geology and Geophysics, Chinese Academy of Sciences. A 15 kV, 20nA beam was focused to diameter 1–5 μm for minerals and 10 μm for melt. Na and K were counted in the first pass to reduce the problem of Na and K loss during analyses (Morgan and London, 2005).

Subsequently, combined the BSE images of the two run products with other products, with different annealing time obtained by Zhang et al. (2019), the apparent dihedral angles at the amphibole-melt-amphibole triple junctions were measured by the software of "Image J". The apparent dihedral angles were measured from BSE images of the well-polished recovered samples at a magnification of × 2000, as shown in Fig. 1 and Fig. 2. The true dihedral angle of the Amp-Melt-Amp was taken to be the median value of the apparent dihedral angle distribution (Stickels and Hucke, 1964). Theoretically, according to previous studies, the measurements error of the apparent dihedral angle is based on a 95 % confidence around the population median (Riegger and van Vlack, 1960; Terasaki et al., 2005). But a small number (<100) of dihedral angle measurements is far from adequate for the determination of the true dihedral angle and the confidence limit. Hence, to obtain an unbiased result, there were hundreds of times random two-dimension-cut measurements in each observation, only in this way could it guarantee a no preselection and no orientation apparent measurement.

3. Results

3.1. Experimental products

Including the experimental products of Zhang et al. (2019), BSE images and electron microprobe analysis of six samples were collected (Fig. 1). Table 2 shows the major mineral phases and chemical composition analysis of amphibole (Amp) and melt (Melt) in the experimental products.

Experimental phases are predominated by Amp and glass melt. According to BSE images, Amp crystals are with distinct boundaries against melts and easily observed (Fig. 1), crystals maintain about 35–58 % in the melt refers to the previous CSD studies by Zhang et al. (2019). The major element analysis of experimental products was then carried out, the compositions of amphiboles and melts are shown in Table 2, proving that the two main components in experimental products are Amp and Melt. Therefore, the experimental products have typical two-phase characteristics, providing an unsophisticated measurement environment for the follow-up apparent dihedral angle measurement.

3.2. Apparent dihedral angle statistics

Apparent dihedral angle measurements were carried out by the software of "Image J". According to BSE images, grains in the melt were gradually squeezed together in the crystallization, therefore the measurement of the apparent dihedral angle is to determine the angle between crystal boundaries via BSE images. The angle measurements were realized by identifying the color difference between the crystal boundaries and the melt, a branch of the melt in the crystals, then fed into the software as angle. During the measurement, to avoid the recognition error of angle, angles were adopted by artificial judgement then sent to the software for automatic measurement. There would be a few degrees of error in each measurement according to Holness (2005). However, the apparent dihedral angle is a characterization of the reasonable approximation of the true dihedral angle, or the measuring error could have little effect on the observed distribution if less than 2° (Jurewicz

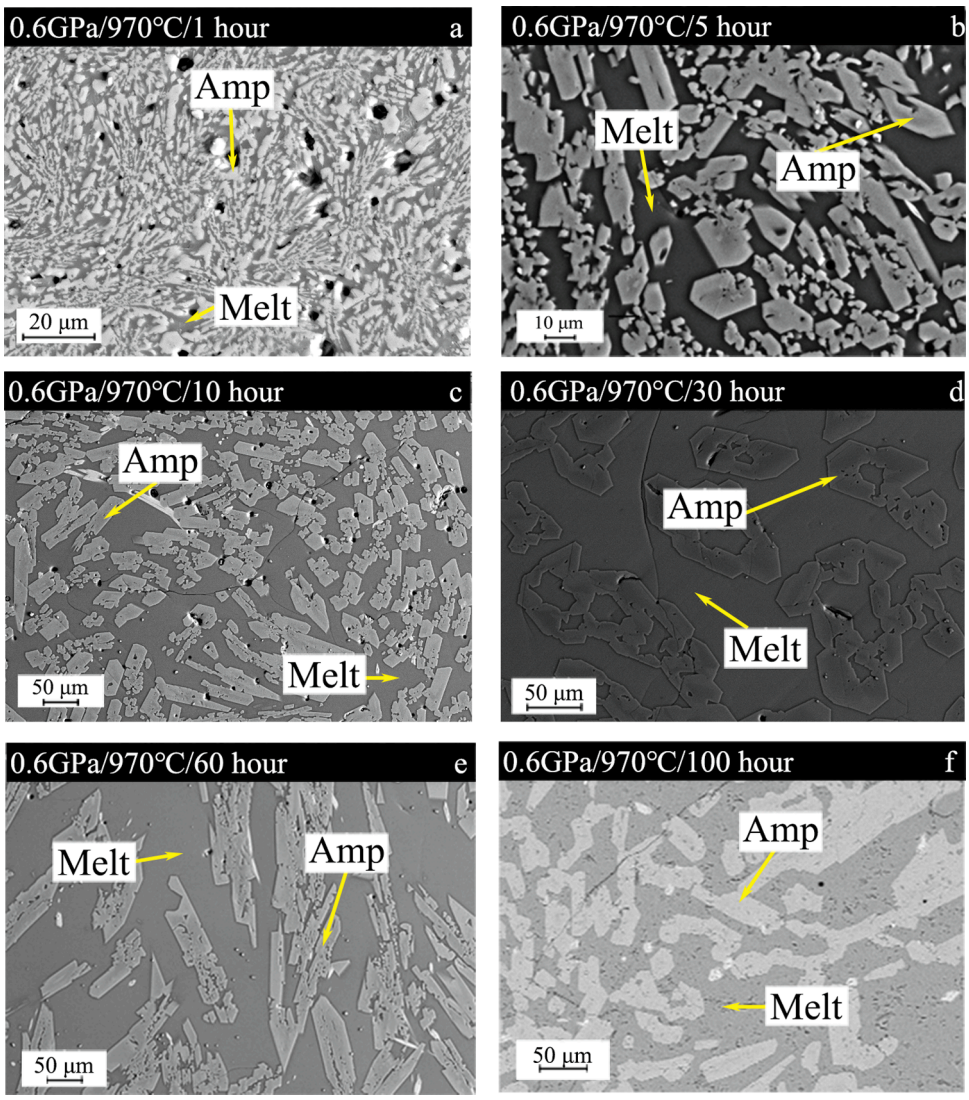

Fig. 1. BSE images of run productions with annealing time of 1 h (a), 5 h (b), 10 h (c), 30 h (d), 60 h (e), and 100 h (f). (a), (c), (e) and (f) are referred from (Zhang et al., 2019), Amp represents amphibole.

and Jurewicz, 1986). So, in order to eliminate the statistical deviation caused by measurement errors as much as possible, more than 600 apparent dihedral angle measurements were made in each annealing time experimental product (Supplemental Table S1).

As shown in Fig. 2, in the annealing time BSE images, crystals have distinct boundaries against melt, which provides the apparent dihedral angle measurement a clear, sharp, and obvious angle between the two crystals, as indicated by the arrows. Drawing from the zoom-in images, the crystals seem to get longer and longer with the increasing annealing time. Subsequently, after the randomly hundreds of measurements, the distributions of apparent dihedral angles are shown in Fig. 3, and Table 3 shows the statistical results of the apparent dihedral angle.

4. Discussion

4.1. Compared with previous studies

Previous studies indicated that the dihedral angle is able to quantify the melt connectivity or to quantify the interfacial energy per unit area of the solid–solid/liquid interface by the grain curvatures (Bulau et al., 1979; Lupulescu and Watson, 1999; von Bargen and Waff, 1986). The dihedral angle distributions will always tend to an equilibrium state with a consistent trend of the median-standard deviation (Hunter and McKenzie, 1989; Liu and German, 2001; Walte et al., 2007). In the other hand, according to Lupulescu and Watson (1999), the apparent dihedral angle could provide a satisfactory indication of the (3-D) dihedral angle distribution, even though it appears a significantly broader than the theoretical distribution with a larger standard deviation (Lupulescu and Watson, 1999).

Moreover, Holness et al. (2005) argued that there is a parabola-like distribution if projecting the median and standard deviation onto a 2-D graph and further concluded the trend curve between the median-standard deviation and the textural equilibrium state (Holness et al., 2005), as shown as the gray dash-line in Fig. 4.

According to Holness et al. (2005), impingement, as one of the typical disequilibrium states, has two trends in the development toward equilibrium: melt-present equilibrium and solid-state equilibrium (Fig. 4), depending on the crystal size, distribution, and the number of initial populations in the melt. From the perspective of median-standard deviation trend, the process from impingement to melt-present equilibrium is usually accompanied by the reduction of median and standard deviation, with a relatively high melt connectivity; and the alternative side, in the process to solid-state equilibrium, the median will increase accompanied with the decrease of standard deviation, and melt connectivity will decrease due to textural coarsening, size enlarging, and the closer arrangement of grains. In summary, it is possible to differentiate

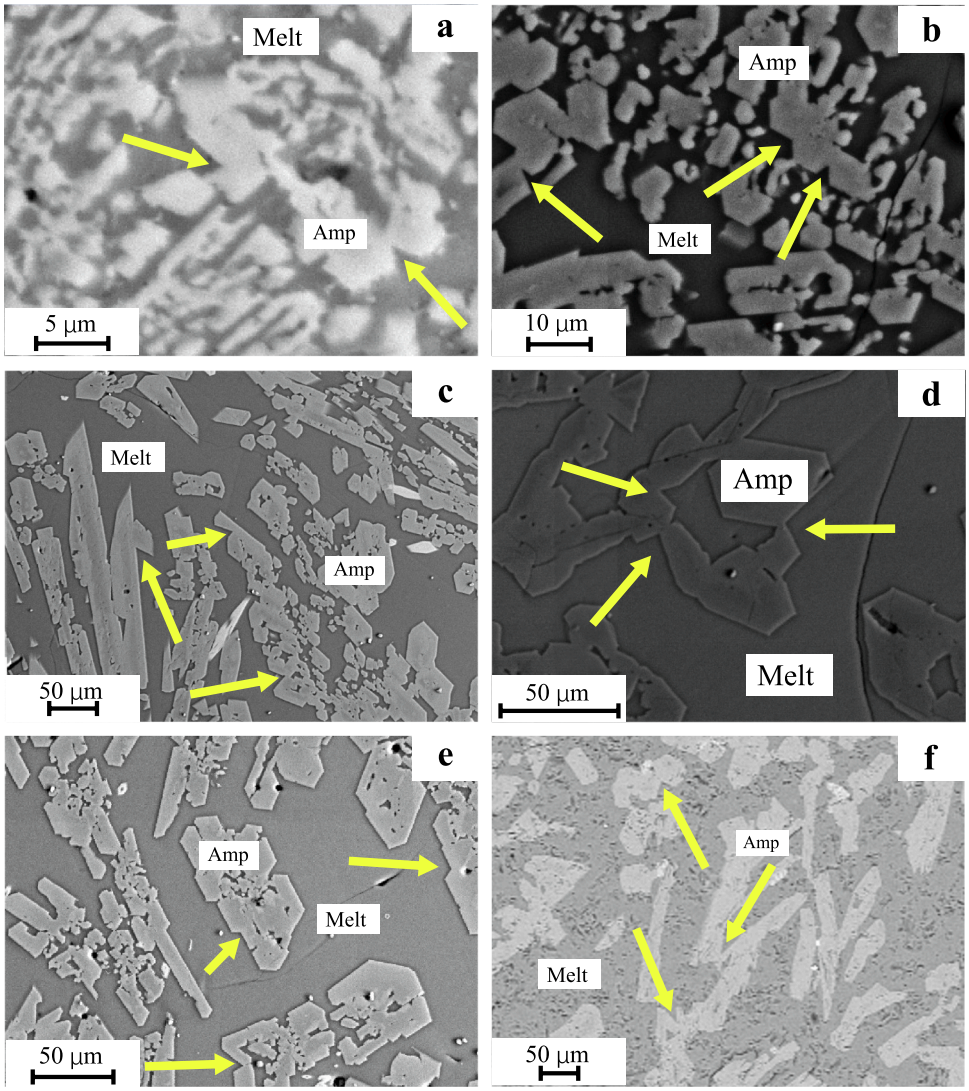

Fig. 2. BSE image of amphibole-melt sample with annealing time of 1 h (a), 5 h (b), 10 h (c), 30 h (d), 60 h (e), and 100 h (f). Arrows indicate the apparent dihedral angles, where amphibole grains were surrounded by melt, have rhombic structure with clear boundaries.

Table 2
Major elements of amphibole and melt of run products.[a]

Run	1		2		3		4		5		6	
n [b]	Amp(5)	Melt(16)	Amp(5)	Melt(9)	Amp(12)	Melt(15)	Amp(8)	Melt(15)	Amp(9)	Melt(11)	Amp(5)	Melt(7)
SiO_2[c]	41(1)	55.5(9)	39(3)	58.2(7)	40(1)	58.5(7)	41.2(4)	52(1)	41(1)	56.1(8)	40.9(7)	58.4(6)
Al_2O_3	13.2(3)	16.3(5)	13.6(8)	19.4(1)	13.4(6)	18.3(2)	14.0(3)	18.0(4)	12.3(2)	17.1(1)	13.5(4)	18.3(2)
TiO_2	3.6(5)	1.1(1)	4.2(3)	0.56(6)	4.0(5)	0.50(4)	3.1(3)	1.53(9)	4.0(5)	1.2(1)	3.5(4)	0.82(6)
Cr_2O_3	0.02(1)	0.01(0)	0.03(2)	0	0.04(2)	0	0.06(2)	0	0.06(2)	0.01(0)	0.2(1)	0.08(8)
MgO	10.4(6)	1.7(1)	10(1)	1.6(1)	11(1)	1.3(1)	17.3(9)	3.1(2)	13.2(7)	1.7(1)	10.9(5)	1.20(8)
NiO	0.02(1)	0.01(0)	0.02(1)	0	0.02(1)	0	0.02(2)	0	0.05(2)	0	0.02(2)	0.02(1)
FeO	14.1(4)	9.0(5)	10.8(3)	5.5(2)	13.3(8)	6.5(2)	7.4(6)	7.3(5)	11.1(8)	7.7(2)	14.0(7)	6.9(2)
MnO	0.18(3)	0.16(3)	0.15(3)	0.12(2)	0.17(3)	0.13(2)	0.12(1)	0.13(2)	0.14(2)	0.16(1)	0.18(5)	0.13(4)
CaO	10.9(5)	4.2(3)	10(1)	4.1(2)	11.6(5)	5.3(3)	9.6(6)	8.0(5)	11.8(4)	6.5(3)	10.3(2)	4.1(2)
Na_2O	2.9(2)	4.3(5)	3.3(1)	6.3(1)	2.9(1)	4.9(1)	2.86(8)	1.7(2)	2.8(1)	4.3(1)	2.82(7)	5. 1(2)
K_2O	1.0(2)	4.1(3)	0.9(1)	2.98(7)	0.7(1)	2.3(1)	0.58(5)	3.8(1)	0.7(1)	2.0(1)	1.0(2)	1.21(4)
Total	97.24	96.33	93.85	98.77	97.68	97.68	96.23	95.78	97.29	96.73	97.24	96.20

[a] Experimental Runs correspond to Table 1 and Run No 1, 3, 5, and 6 are referred from (Zhang et al., 2019).
[b] Number of analyses.
[c] Wt.% oxides, values in parentheses are standard deviations, thus, 41(1), 55.5(9), 0.14(9) should be read as 41 ± 1, 55.5 ± 0.9, 0.14 ± 0.09, respectively.

melt-bearing equilibrium and impingement textures by true 3-D dihedral angle populations (Holness et al., 2005).

After all, with the increase of annealing time, the melt would tend to an equilibrium state. Hence the early stage of magma crystallization in this study could be understood as: initial crystallization (1 h annealing) – impingement state (5 h, 10 h, 30 h) – near-equilibrium (60 h, 100 h).

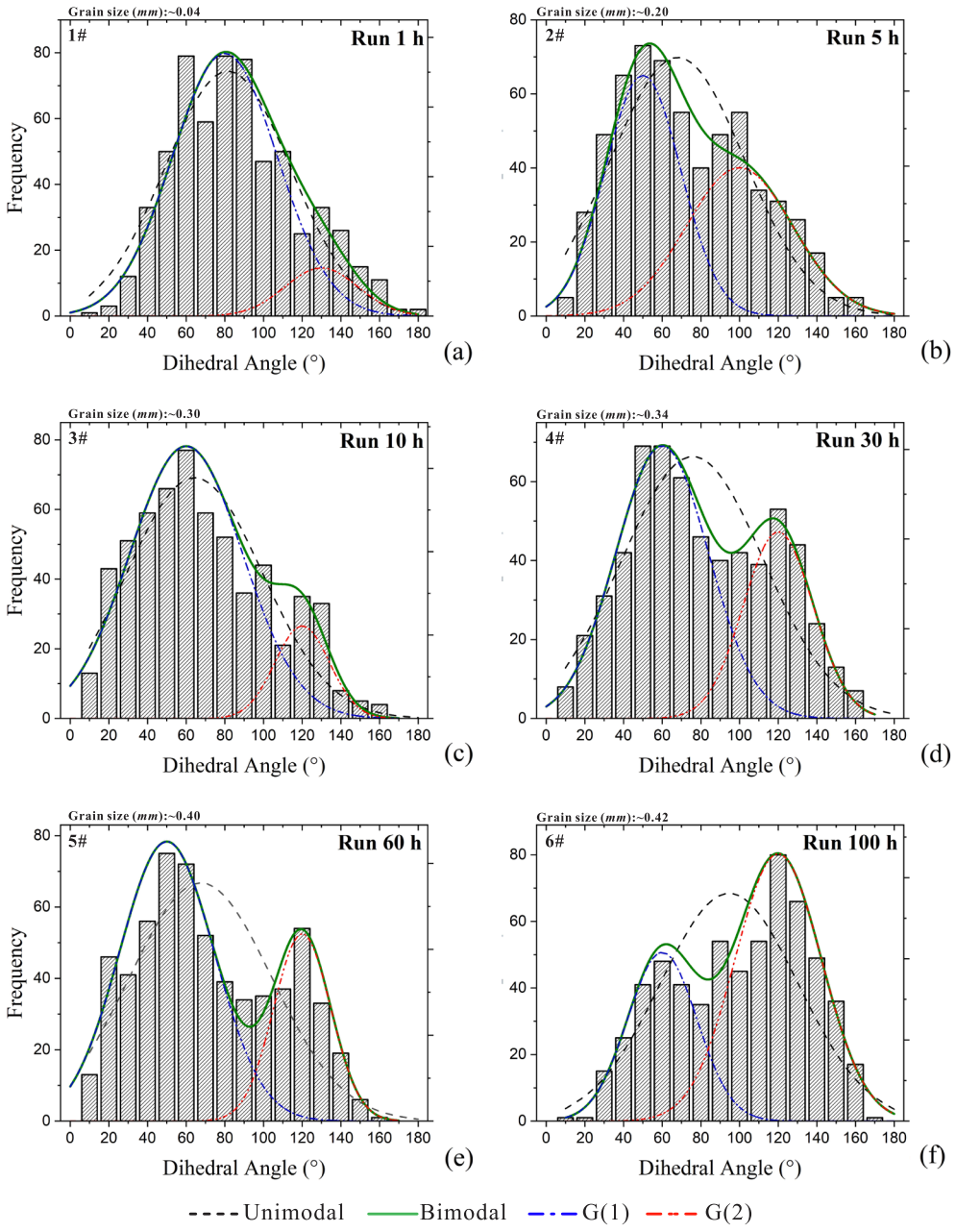

Fig. 3. Amp-melt apparent dihedral angle distributions at 0.6 GPa and 970 °C with annealing time of 1 h (a), 5 h (b), 10 h (c), 30 h (d), 60 h (e), and 100 h (f), respectively. The legend of the figures on the bottom: black long dotted line, normal distribution according to classical normal distribution; green solid line, superposition curve of two Gaussian curves; blue dotted line, the first Gaussian distribution curve (G(1)) on the left; and the red double dotted line, the second Gaussian curve (G(2)) on the right.

Table 3
Statistical parameters of the apparent dihedral angles.

Annealing time (h)	1	5	10	30	60	100
Counts	605	606	606	609	613	609
Median (°)	78.0	62.0	59.7	70.7	61.3	99.8
Expectation (°)	81.5	68.0	64.4	75.8	67.5	94.6
Standard Deviation (°)	31.9	34.1	34.5	36.2	36.2	35.0
Range (°)	9.7–174.8	7.0–157.8	3.6–158.2	4.0–157.4	4.2–152.8	8.7–160.6

However, as shown in Fig. 4, the trend of the median-standard deviation with annealing time of this study (black arrow) does not conform to the mode summarized by Holness et al. (2005). In this study, the median apparent dihedral angle is at a high value (~77°) at the beginning (1 h), the standard deviation is also relatively low. As the crystallization time increases (5 h – 30 h), the crystal distribution in the melt gradually balances to a median of about 60°, but the standard deviation is also on the rise at the same time. With the further increasing crystallization time (60 h – 100 h), the median increases with a decreased standard deviation.

Compared with Holness et al. (2005), it is obvious that the crystallization time in the laboratory is far from the natural rock samples. In other words, this pattern does not seem to be suitable for the early-stage crystallization in magma. Almost all the statistical data conforming to cumulus crystal growth patterns were collected from true dihedral angle measurements in natural rock samples (Terasaki et al., 2005). However,

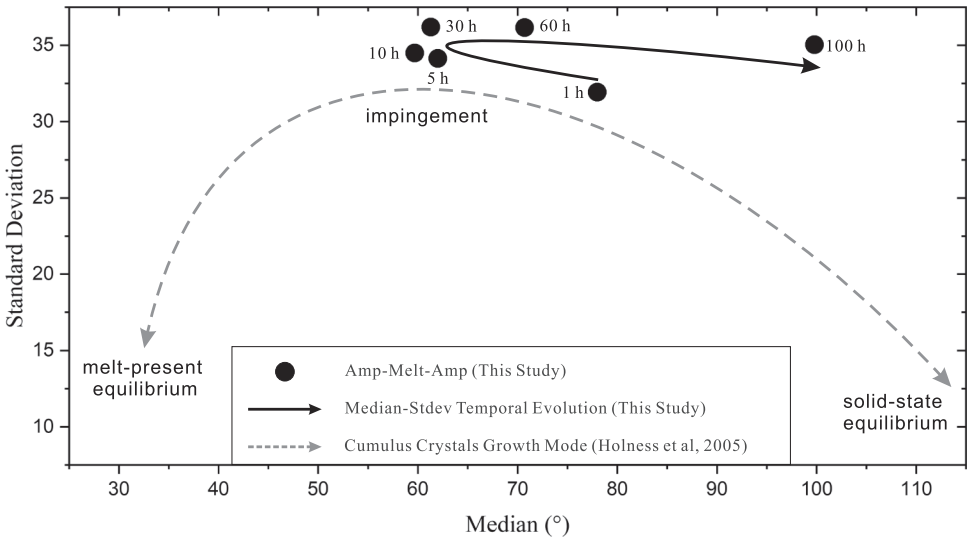

Fig. 4. Median-standard deviation distribution of this study vs Cumulus crystal growth mode from (Holness et al., 2005).

Elliott et al. (1997) believed that situations were more complicated in natural rocks, it was not uniform in random distribution of grains, sometimes led to a high/low median-standard deviation in one snapshot. Moreover, the cause of this situation has little relationship with nucleation rates or distributions in the further simulation experiments, besides the disequilibrium itself, only anisotropy could lead to the result (Elliott et al., 1997).

In addition, the statistical results of the apparent dihedral angle in previous work usually have strong normality (Jurewicz and Jurewicz, 1986; Price et al., 2006; Wark et al., 2003; Yoshino et al., 2006), that is the reason why it is effective to take median value as true dihedral angle in the apparent dihedral angle measurement (Ono et al., 2002; Terasaki et al., 2002). As shown in Fig. 3, the distribution of apparent dihedral angle in this study, different from previous studies, deviates dramatically from the normal distribution. Hence, before further analysis, it needs a prior normality test to check if the data is normal or not.

For the normality test, if obeys the normal distribution, the null hypothesis will be accepted when the observed value is less than the expected value, with a significance level (P value) of 0.05, by this time the data is called a normal distribution (Yazici and Yolacan, 2007). However, one specific method may only reflect the normality of the data to one certain extent, so it is necessary to use a cross validation by two or more normality tests (Mishra et al., 2019). The Kolmogorov–Smirnov (K-S) (Stephens, 1974) and Chi-squared (C-s) (Nikulin, 1973) methods are adopted to test the normality for large sample data (greater than600 samples). As shown in Table 4, the null hypothesis to be normal distribution will only be accepted that, the maximum difference between the observed and the expected values are no more than 0.055 according to the K-S method; meanwhile the cumulative frequencies at freedom degrees of 17 should be less than 8.672 by using the C-s method.

Table 4
Normal distribution test.

Run	1 (1 h)	2 (5 h)	3 (10 h)	4 (30 h)	5 (60 h)	6 (100 h)
$D\|_{max}$ / K-S[a]	0.020	0.069	0.060	0.063	0.076	0.078
$D\|^{b}_{0.05}$	0.055	0.055	0.055	0.055	0.055	0.055
Null hypothesis	accept	reject	reject	reject	reject	reject
$\chi^2_{df=17}$ / C-s[a]	69.357	67.994	82.138	77.712	115.469	104.460
$\chi^2\|^{b}_{0.05,\ df=17}$	8.672	8.672	8.672	8.672	8.672	8.672
Null hypothesis	reject	reject	reject	reject	reject	reject

[a] $D|_{max}$ and $\chi^2|_{df=17}$ are the maximum difference between assumed normal distribution and statistics for the Kolmogorov–Smirnov (K-S) and Chi-squared (C-s) methods, respectively. 17 degrees of freedom (df = 17) corresponds to 18 intervals of data classification. Significance level α is set to 0.05, so the criterion of rejection is to test if $D|_{max}$ or $\chi^2|_{df=17}$ were greater than 5 %.

[b] $D|_{0.05}$ and $\chi^2|_{0.05,\ df=17}$ are the 5 % statistical difference between assumed normal distribution and statistics if the significance level α is set to 0.05.

In terms of normality test results, except the 1-h-annealing experimental product (K-S test in Run 1), apparent dihedral angle statistics of other experimental products hardly have the characteristics of the normal distribution. Since then, with the increase of bimodality, the median-standard deviation trend in this study was growing deviated from the model summarized by Holness et al. (2005).

As mentioned before, the main solid phase in our experimental products is amphibole. The apparent dihedral angle distribution of the 1 h product maintained a unimodal shape (Fig. 3a), which is consistent with the normality test too (Table 4). After that, because of the energetically favorable orientation in amphibole, the grains with uniform curvature will gradually elongate during the coarsening process (Higgins, 2010). Ideally, the longer the crystallization time is, the stronger the amphibole boundary anisotropy will be (Liu and German, 2001; Riegger et al., 1980). Furthermore, the crystal size distributions (CSDs) of amphibole with annealing time of 1 h, 10 h, 60 h and 100 h (Zhang et al., 2019) indicate that the average lengths of amphibole crystal long axes increase significantly with the increase of annealing time in the isobaric process, and the change of the long axis of the crystal gradually dominates the growth rate of amphibole. Therefore, the anisotropy of amphibole plays a key role in the crystal growth during the early-stage magma crystallization, which might dramatically affect the shape of the crystal, then the distribution of dihedral angle.

4.2. *Bimodal distribution of the apparent dihedral angle and the effect of anisotropy*

Taking 10° as the grouping interval, the distribution of apparent dihedral angle (Fig. 3) has two obvious characteristics: 1) the distribution presents an increasingly distinct bimodal characteristics, and 2) the median values of bimodality gradually stabilize at 60° and 120°.

Mathematically, one bimodal curve is often written as a weighted sum of two unimodal Gaussian functions according to the strength of the statistics (Pieri et al., 2006), in the form of:

$$F = w_1 G(\mu_1, \sigma_1) + w_2 G(\mu_2, \sigma_2)$$

where the weight (w) is used to fitting the intensity, μ and σ is median

and standard deviation of the separate Gaussian function, respectively. However, in this study, for the sake of simplicity, the intensity of the unimodal Gaussian function is not concluded in the discussion, our focus is mainly on the parameters of the function itself, which are statistically relevant.

Firstly, the bimodal distributions were split into two unimodal distributions, as shown in dotted dash lines in Fig. 3. The two curves on the left and right are marked as "the first unimodal distribution, G(1)" and "the second unimodal distribution, G(2)", then the variation trends of their median values and standard deviations with the increase of annealing time are obtained, too (Table 5 and Fig. 5).

In the median-annealing time relationships (Fig. 5a), the curves are disturbed with the increase of annealing time, with the medians ranging from 50° to 80° for G(1) and 100° to 130° for G(2). Moreover, the medians of the two unimodal Gaussian functions are complementary to each other, the final values of two curves are 60° and 120°, respectively. From the perspective of the Amp crystals, according to its cleavage characteristics, the initial shape will be rhombus from the beginning of the formation (120° of each inner Angle). Along with the crystal growth, the crystals will elongate symmetrically to one certain orientation. In this case, if the position of one crystal was relatively unchanged, the angle between contact surface and the "elongated crystal" boundary would become acute on one side and obtuse on the other side. That is to say, if it is 60° on one side, there will be an angle of 120° on the other side, complementary to each other.

Secondly, the trend of the standard deviation against the annealing time (Fig. 5b) reflects the concentration of the dihedral angle. Referred from the crystal growth mode (Fig. 4), statistically, the standard deviation will not only reflect the concentration of the data, but also the changes in crystal growth. Generally, it is considerable that in case there exists a small standard deviation, there shall be more cohesive inside the crystals, in this situation there might be a larger grain interfacial energy (Holness et al., 2005). Conversely, if the standard deviation is large, the crystal growth direction should be dominated by the stronger surface energy.

Ideally, the dihedral angle of isotropic minerals under thermal equilibrium would tend toward 120° at solid-state equilibrium, where the shape and scale of grain are mostly governed by the principle of interfacial energy minimization (Gabrisch et al., 1998; Laporte and Watson, 1995). But for anisotropic minerals, the dihedral angle will not be a specific value due to the different surface energy from crystal planes (Cmíral et al., 1998; Holness and Vernon, 2015). This explains the different standard deviation development trends with increasing annealing time (Fig. 5b). The downward trend standard deviation of G(1) reflects the growth directions of grains that were affected by interfacial energy, and the upward trend standard deviation of G(2) reflects the growth orientations of grains dominated by surface energy.

After all, dihedral angle is a function of surface energy, that the grain boundary energy and the interfacial energy should change along with crystallization, and finally achieve the minimum Gibbs free energy in system (Yoshino, 2005; Yoshino et al., 2006), while the interface of the anisotropy crystal would be a faceting plane rather than constant curvature. However, the interfaces were almost flat plane even at 100 h system (Fig. 2f), indicating that the Gibbs free energy of the Amp crystal in the 100 h melt had not yet reached a minimum, or a texture equilibrium.

4.3. Texture evolution with time

According to Holness et al. (2005) (Fig. 4), the standard deviation usually maintains a relatively low level, the final median dihedral angles will generally be around 30° and 120° for melt-present equilibrium and solid-state equilibrium, respectively, even though the impingement process generates a relatively high deviation (~25°) (Holness et al., 2005).

However, in this study, the situation is quite different according to the experimental products. After statistical analysis, we found impingement state reached in the 5 h, 10 h and 30 h experimental products after the 1-hour initial crystallization (Fig. 1b-1d, Figs. 5, 6). As the annealing time further increased to 60 h and 100 h, the impingement state was gradually tending to the melt-present equilibrium (Fig. 1e, 1f, Fig. 6). That is to say, the longer the crystallization time is, the more equilibrium in the melt-amphibole system.

Because of the clearer bimodal characteristics of the apparent dihedral angle distribution with the increasing annealing time, it is appropriate to use two-Gauss-function-fitting (G(1) and G(2)) to reveal the features of the distributions, except the 1 h sample (Fig. 3). As shown in Fig. 6, the two curves (blue and red) show the variation trend of the median-standard deviation of G(1) and G(2). In further analysis, by combining with Fig. 5 and Fig. 6, it shows great differences between the median-standard deviation evolutions of G(1) and G(2) in the early crystallization. For G(1), the median value gradually stabilizes at 60° with increasing annealing time, accompanies with a reduction of standard deviation (reduces to about 18° in the 100 h sample); for G(2), the median value is stabilized at 120° after the 10 h annealing, with a gradually decreased standard deviation, but it slightly rebounds to 22° when the annealing time reaches 100 h. Therefore, the median-standard deviation with the growth of textural equilibrium in the early stage of magma crystallization is no longer a unidirectional change.

In addition, it is important to find out whether the apparent dihedral angle distribution is time related, or anisotropy related after all. Will the distribution of apparent dihedral angle be unimodal again after annealing time over 100 h? The future work will focus on the actual dependent pattern in a longer annealing time crystallization (more than 100 h), take both the annealing time and anisotropy of crystallization into account. However, in this study, the conclusion could be drawn in mentioning several prerequisites, namely the two-phase melt, amphibole the main minerals, sufficient space, and time for the crystallization, etc. Once met the conditions (the main experimental conditions in this study), it can be considered that the dominant anisotropy of amphibole crystals in the crystallization process eventually leads to the bimodal characteristics in the apparent dihedral angle distribution. In other words, the highly anisotropy of amphibole seems to dominate the dihedral angle distribution pattern at the early stage of crystallization in the amphibole-melt system.

4.4. Implication

In previous studies, it is generally considered that the crystal growth in the early evolution of magma is a random, natural and no specific orientational process. So, the issues like permeability, crystal texture, and melt connectivity are more discussed under equilibrium state or even a completely solidary melt. In fact, the bimodality caused by anisotropy may have played a key role in the early crystallization of

Table 5
Statistical parameters of bimodal distributions for the apparent dihedral angle.

Run #		1	2	3	4	5	6
Left Gaussian distribution	Median (°)	80.0	50.0	60.0	60.0	50.0	60.0
	Standard Deviation	27.16	19.58	29.11	24.02	24.43	17.89
Right Gaussian distribution	Median (°)	130.0	100.0	120.0	120.0	120.0	120.0
	Standard Deviation	18.91	27.91	14.14	18.05	14.74	22.34

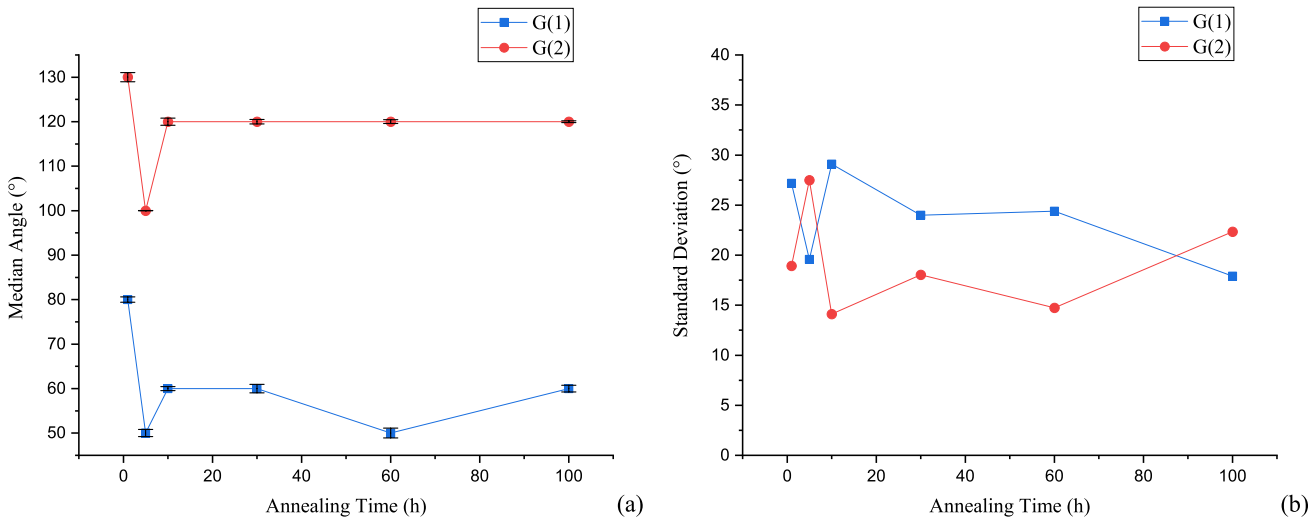

Fig. 5. Median and standard deviation value of the bimodal distributions. (a) In median curves, the median of G(1) stabilizes at 60° with fluctuation and the median of G(2) stays at 120° stably. (b) Standard deviation curves, the standard deviations of G(1) decrease with increasing annealing time and the standard deviations of G (2) fluctuate with increasing annealing time and reach a higher value after annealing for 100 h.

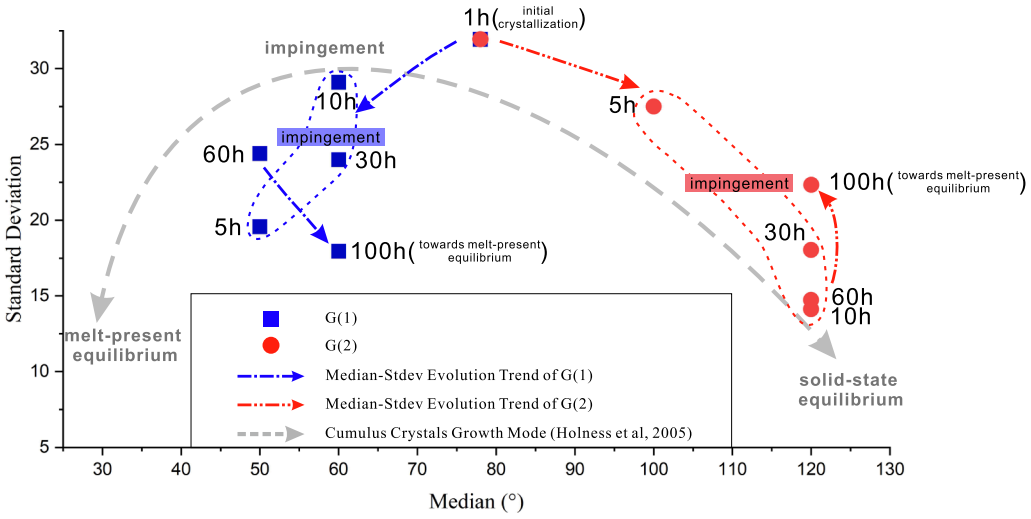

Fig. 6. Schematic diagram of the texture evolution of amphibole-melt dihedral angle during early stage of magma crystallization. Blue square and red dot in figure represent G(1) and G(2) separately from the statistical results. With increasing annealing time, the "bimodal" characteristics of apparent dihedral statistics becomes clearer, the median values of the two separated Gaussian distributions show a stable trend, along with an obvious downward trend of standard deviations.

magma, according to the apparent dihedral angle distribution. Hence, the bimodal distribution of apparent dihedral angle provides another evidence to support the crystal growth in the two-phase melt from another perspective, it is of geological significance to understand the origin of the connectivity and permeability of magma from the early-stage development of anisotropic crystals.

5. Conclusions

The apparent dihedral angle distribution is the key to study the texture development during magma crystallization. In this study, we carried out two additional crystallization experiments in amphibole-melt system with a single variable of annealing time. Then the apparent dihedral angle distributions of the two experimental products and four previous experimental products were analyzed to investigate the texture evaluation in early crystallization. The results indicate that the apparent dihedral angle presents a gradually obvious bimodal distribution with the increase of annealing time, which needs two Gaussian functions to fit. After all, the high anisotropy of amphibole is the main cause of the bimodal characteristics. In the further analysis, the textural evolution in the early crystallization shows a different trend of the median-standard deviation of the apparent dihedral angle comparing to the one summarized by predecessors.

Funding

This work was supported by the Joint Research Fund in Huge Scientific Equipment under cooperative agreement between NSFC and CAS [U2032118], the Science and Technology Foundation of Guizhou Province [QKHJC-ZK[2021]YB202], and the Development Project of Young Science and Technology Talents in Guizhou Province [QJH-KY [2022]324].

CRediT authorship contribution statement

Qizhe Tang: Visualization, Writing – original draft, Writing – review & editing. **Bo Zhang:** Visualization, Investigation, Data curation, Software, Formal analysis, Funding acquisition. **Wenge Zhou:**

Conceptualization, Methodology, Resources, Formal analysis, Supervision, Funding acquisition.

Declaration of Competing Interest

The authors declare that they have no known competing financial interests or personal relationships that could have appeared to influence the work reported in this paper.

Data availability

Data will be made available on request.

Acknowledgements

We thank two anonymous reviewers for constructive reviews. We express our gratitude to Dr. Hu Xianxu, Dr. Jiang Neng, Dr. Li Peng for their helpful assistance in experiments, the constructive comments and discussions are of great help to us in improving our manuscript. We thank our funders for funding this study.

Appendix A. Supplementary material

Supplementary data to this article can be found online at https://doi.org/10.1016/j.jseaes.2022.105405.

References

Bulau, J.R., Waff, H.S., Tyburczy, J.A., 1979. Mechanical and thermodynamic constraints on fluid distribution in partial melts. J. Geophys. Res. Solid Earth 84 (B11), 6102. https://doi.org/10.1029/JB084iB11p06102.

Cmíral, M., Gerald, J.D.F., Faul, U.H., Green, D.H., 1998. A close look at dihedral angles and melt geometry in olivine-basalt aggregates: a TEM study. Contrib. Miner. Petrol. 130 (3-4), 336–345.

Elliott, M.T., Cheadle, M.J., Jerram, D.A., 1997. On the identification of textural equilibrium in rocks using dihedral angle measurements. Geology 25 (4), 355. https://doi.org/10.1130/0091-7613(1997)025<0355:OTIOTE>2.3.CO;2.

Gabrisch, H., Dahmen, U., Johnson, E., 1998. In situ measurement of dihedral angles at liquid grain boundary inclusions. Microsc. Res. Tech. 42 (4), 241–247.

Higgins, M.D., 2010. Textural coarsening in igneous rocks. Int. Geol. Rev. 53 (3-4), 354–376.

Holness, M.B., 2005. Melt-Solid Dihedral Angles of Common Minerals in Natural Rocks. J. Petrol. 47 (4), 791–800.

Holness, M.B., Cheadle, M.J., McKenzie, D.A.N., 2005. On the Use of Changes in Dihedral Angle to Decode Late-stage Textural Evolution in Cumulates. J. Petrol. 46 (8), 1565–1583.

Holness, M.B., Nielsen, T.F.D., Tegner, C., 2006. Textural maturity of cumulates: a record of chamber filling, liquidus assemblage, cooling rate and large-scale convection in mafic layered intrusions. J. Petrol. 48 (1), 141–157.

Holness, M.B., Vernon, R.H., 2015. The Influence of Interfacial Energies on Igneous Microstructures. In: Charlier, B., Namur, O., Latypov, R., Tegner, C. (Eds.), Layered Intrusions. Springer, Netherlands, Dordrecht, pp. 183–228.

Holness, M.B., Tegner, C., Nielsen, T.F., Stripp, G., Morse, S.A., 2007. A textural record of solidification and cooling in the Skaergaard intrusion, East Greenland. J. Petrol. 48, 2359–2377.

Holness, M.B., Stock, M.J., Geist, D., 2019. Magma chambers versus mush zones: constraining the architecture of sub-volcanic plumbing systems from microstructural analysis of crystalline enclaves. Philos. Trans. A Math. Phys. Eng. Sci. 377 (2139), 20180006. https://doi.org/10.1098/rsta.2018.0006.

Hunter, R.H., McKenzie, D., 1989. The equilibrium geometry of carbonate melts in rocks of mantle composition. Earth Planet. Sci. Lett. 92, 347–356.

Ikeda, S., Toriumi, M., Yoshida, H., Shimizu, I., 2002. Experimental study of the textural development of igneous rocks in the late stage of crystallization: the importance of interfacial energies under non-equilibrium conditions. Contrib. Miner. Petrol. 142, 397–415.

Jurewicz, S.R., Jurewicz, A.J.G., 1986. Distribution of apparent angles on random sections with emphasis on dihedral angle measurements. J. Geophys. Res. Solid Earth 91, 9277–9282.

Laporte, D., Watson, E.B., 1995. Experimental and theoretical constraints on melt distribution in crustal sources: the effect of crystalline anisotropy on melt interconnectivity. Chem. Geol. 124, 161–184.

Liu, J., German, R.M., 2001. Microstructure effect on dihedral angle in liquid-phase sintering. Metall. Mater. Trans. A 32, 165–169.

Lupulescu, A., Watson, E.B., 1999. Low melt fraction connectivity of granitic and tonalitic melts in a mafic crustal rock at 800 C and 1 GPa. Contrib. Miner. Petrol. 134, 202–216.

Mishra, P., Pandey, C.M., Singh, U., Gupta, A., Sahu, C., Keshri, A., 2019. Descriptive statistics and normality tests for statistical data. Ann. Card. Anaesth. 22, 67–72.

Morgan, G.B., London, D., 2005. Effect of current density on the electron microprobe analysis of alkali aluminosilicate glasses. Am. Mineral. 90, 1131–1138.

Nikulin, M., 1973. Chi-squared test for normality, Proceedings of the International Vilnius Conference on Probability Theory and Mathematical Statistics, pp. 119-122.

Ono, S., Mibe, K., Yoshino, T., 2002. Aqueous fluid connectivity in pyrope aggregates: water transport into the deep mantle by a subducted oceanic crust without any hydrous minerals. Earth Planet. Sci. Lett. 203, 895–903.

Pieri, L., Bittelli, M., Pisa, P.R., 2006. Laser diffraction, transmission electron microscopy and image analysis to evaluate a bimodal Gaussian model for particle size distribution in soils. Geoderma 135, 118–132.

Price, J.D., Wark, D.A., Watson, E.B., Smith, A.M., 2006. Grain-scale permeabilities of faceted polycrystalline aggregates. Geofluids 6, 302–318.

Riegger, H., Pask, J., Exner, H., 1980. Sintering processes. Plenum Press, New York, NY.

Riegger, O., van Vlack, L., 1960. Dihedral angle measurements: Metallurgical Society Transactions. AIME 933–935.

Stephens, M.A., 1974. EDF Statistics for Goodness of Fit and Some Comparisons. J. Am. Stat. Assoc. 69, 730–737.

Stickels, C.A., Hucke, E., 1964. Measurement of dihedral angles. Trans. Metall. Soc. AIME 230, 795–1000.

Terasaki, H., Rubie, D., Frost, D., 2002. Estimation of the timescale for textural equilibrium between liquid iron-sulfide and solid silicate under high pressure, AGU Fall Meeting Abstracts, pp. MR52A-1007.

Terasaki, H., Frost, D.J., Rubie, D.C., Langenhorst, F., 2005. The effect of oxygen and sulphur on the dihedral angle between Fe–O–S melt and silicate minerals at high pressure: Implications for Martian core formation. Earth Planet. Sci. Lett. 232, 379–392.

Vicenzi, E., Rapp, R., Watson, E., 1988. Crystal/melt wetting characteristics in partially molten amphibolite. J. Eos Tansform. AGU 69.

von Bargen, N., Waff, H.S., 1986. Permeabilities, interfacial areas and curvatures of partially molten systems: Results of numerical computations of equilibrium microstructures. J. Geophys. Res. Solid Earth 91, 9261–9276.

Waff, H.S., Bulau, J.R., 1979. Equilibrium fluid distribution in an ultramafic partial melt under hydrostatic stress conditions. J. Geophys. Res. Solid Earth 84, 6109–6114.

Walte, N.P., Becker, J.K., Bons, P.D., Rubie, D.C., Frost, D.J., 2007. Liquid-distribution and attainment of textural equilibrium in a partially-molten crystalline system with a high-dihedral-angle liquid phase. Earth Planet. Sci. Lett. 262, 517–532.

Wark, D.A., Williams, C.A., Watson, E.B., Price, J.D., 2003. Reassessment of pore shapes in microstructurally equilibrated rocks, with implications for permeability of the upper mantle. J. Geophys. Res.: Solid Earth 108.

Wolf, M.B., Wyllie, P.J., 1991. Dehydration-melting of solid amphibolite at 10 kbar: Textural development, liquid interconnectivity and applications to the segregation of magmas. Mineral. Petrol. 44, 151–179.

Yazici, B., Yolacan, S., 2007. A comparison of various tests of normality. J. Stat. Comput. Simul. 77, 175–183.

Yoshino, T., 2005. Grain boundary wetness of texturally equilibrated rocks, with implications for seismic properties of the upper mantle. J. Geophys. Res. 110.

Yoshino, T., Price, J.D., Wark, D.A., Watson, E.B., 2006. Effect of faceting on pore geometry in texturally equilibrated rocks: implications for low permeability at low porosity. Contrib. Miner. Petrol. 152, 169–186.

Zhang, B., Hu, X., Asimow, P.D., Zhang, X., Xu, J., Fan, D., Zhou, W., 2019. Crystal size distribution of amphibole grown from hydrous basaltic melt at 0.6–2.6 GPa and 860–970 °C. Am. Mineral. 104, 525–535.